Ph.D. Dissertation of Medicine

Optimal Insertion Site of Glenoid Baseplate in Reverse Total Shoulder Arthroplasty

– Anatomical simulation using 3D image processing software –

역행성 인공관절 치환술에서 최적의 관절와 치환물 삽입 위치

– 3차원 영상 처리 소프트웨어를 이용한 해부학적 모사 연구 –

August 2022

Graduate School of Medicine
Seoul National University
Orthopaedic Surgery Major

Hyeon Jang Jeong

Optimal Insertion Site of Glenoid Baseplate in Reverse Total Shoulder Arthroplasty

– Anatomical simulation using 3D image processing software –

지도교수 오 주 한

이 논문을 의학박사 학위논문으로 제출함

2022년 4월

서울대학교 대학원

의학과 정형외과학

정 현 장

정현장의 의학박사 학위논문을 인준함

2022년 7월

위 원 장 강 승 백 (인)

부위원장 오 주 한 (인)

위 원 조 현 철 (인)

위 원 홍 성 환 (인)

위 원 유 재 철 (인)

Abstract

Purpose: Conventionally, the central structure of the baseplate is inserted through the point where the vertical and horizontal axes of the glenoid intersect (conventional insertion site, CIS). However, there is scanty theoretical evidence that CIS has the optimal bone stock. We evaluated the optimal insertion site for the glenoid baseplate through the three-dimensional volumetric measurement of the glenoid bone stock.

Methods: Preoperative computed tomography (CT) images of 30 consecutive reverse total shoulder arthroplasty procedures were analyzed. Three-dimensional image processing software was used to reconstruct CT and volumetrically measure the glenoid bone stock according to the simulated central peg. A simulated central peg was inserted to the medial pole of the scapula from 49 points determined along with the intersect point of the vertical and horizontal axes of the glenoid CIS at 2-mm intervals. The overlapped volume between the simulated central peg and glenoid vault, representing the amount of glenoid bone stock along the passage of the central peg, was then automatically calculated.

Results: The depth of the glenoid vault was 25.5 ± 3.0 mm (range, 19.3-31.5), and the mean overlapped volume between the simulated central peg and the glenoid vault was 623.0 ± 185.8 ml. The optimal insertion site for the bony purchase of the central peg was 2 mm inferior and posterior from the CIS (765.3 ± 157.5).

Conclusion: The optimal insertion site of the baseplate is located 2 mm inferiorly and posteriorly to the CIS. This anatomical information may be used as a reference to determine the optimal insertion site of the baseplate according to an implant of a surgeon's choice.

Keyword: glenoid baseplate, optimal insertion site for glenoid baseplate, reverse total shoulder arthroplasty, three-dimensional volumetric measurement.

Student Number : 2018-35046

Table of Contents

Chapter 1. Introduction

1.1. Study Background

Reverse total shoulder arthroplasty (RTSA) has been first introduced to treat the irreparable rotator cuff tear and/or cuff tear arthropathy, and its indication has expanded to various diseases of the shoulder. It has characteristics that distinguish it from other arthroplasty. While most arthroplasty focus on mimicking and reconstructing normal anatomy and biomechanics of the joint structure, RTSA is aimed at functional reconstruction and uses a completely different morphologic shape of an artificial joint implant from normal anatomy.

The bony structure of the glenohumeral joint consists of ball shape humeral head and shallow, concave glenoid fossa. This anatomical structure allows a wider range of motion than any other joint, but on the contrary, it has the disadvantage of the inherent instability of the joint structure itself (1). Therefore, the stability of the glenohumeral joint depends on the synergy of various static and dynamic stabilizers.

The primary static stabilizers consist of the congruency of the humeral head and glenoid fossa, glenoid labrum, glenohumeral ligaments, joint capsule, and negative intra-articular pressure. However, the static stabilizers are not sufficient to obtain stability of the glenohumeral joint, and the action of dynamic stabilizers is essential. The dynamic stabilizer is the co-ordinance of various muscles including the rotator cuff, deltoid, pectoralis major,

latissimus dorsi, and periscapular muscles (1). The rotator cuff muscles have primary importance as a contraction of the rotator cuff compresses the humeral head into the glenoid and it allows to maintain the center of rotation (COR) of the glenohumeral joint and increase the force necessary to rotate the humeral head during the shoulder motion, and the dynamic stability of rotator cuffs consists of horizontal and vertical muscle balance called 'force coupling' (2).

The horizontal force couple is formed by the subscapularis and infraspinatus-teres minor complex and the vertical force couple is formed by the deltoid and lower rotator cuff complex (3). If the force coupling is disrupted by the extended rotator cuff tear, the vector of the joint reaction force migrated to the outside of the glenoid rim, and the imbalance of this force coupling provokes the anterosuperior migration of the humeral head under increased traction force exerted by the deltoid which acts as an elevator of the humeral head, leading to pseudoparalysis (4-6).

Although the majority of rotator cuff tears can be treated by rotator cuff repair, several rotator cuff tears cannot be reattached to the footprint during attempted repair (7), and retear rate has been reported up to 20-94% (8-10). Furthermore, not all pseudoparalysis can be restored by rotator cuff repair (11, 12). Therefore, the need for a method to solve these problems has emerged, and RTSA was proposed as the solution to the problem that originated from rotator cuff insufficiency.

Grammont et al. introduced the concept of the reversed ball-and-socket joint with four key principles: (1) medialization of the COR, (2) re-tensioning of the deltoid by distalization of humerus, (3) a constant, fixed COR leading to an inherently stable implant, and (4) semi-constrained implant feature with a larger arc of

motion (13, 14).

RTSA modifies the COR of the glenohumeral joint from the center of the humeral head to the center of the glenosphere–baseplate–glenoid interface; the baseplate is inserted into the glenoid vault, and the glenosphere is assembled on the baseplate. Movements around the fixed COR of the RTSA convert the compressive and shear forces into a large compressive vector, and the peak compressive and shear force generated during shoulder motion is reduced in RTSA (15). Therefore, the glenohumeral joint force in abduction decreased, and the pseudoparalysis can be restored (16). Furthermore, in the case of rotator cuff insufficiency the compressive force of the rotator cuff is diminished, and minimization of the ratio of shear to compressive force at the joint increase the stability of the prosthesis (14).

Distalization of the humerus provoke the lengthening of the deltoid and enhance the deltoid efficiency. Medialized COR and distalization of humerus modify the orientation of the deltoid muscle fiber more vertical direction, and the deltoid moment arm is increased compared with native shoulders (15–17). These anatomical and biomechanical changes increase deltoid recruitment that making the deltoid serves as the primary abductor of the shoulder joint (18).

Also, the design characteristics of the RTSA, which consist of a fixed, relatively larger glenosphere, smaller humeral cup, and the congruency of the radius of curvature between the glenosphere and humeral cup, improved the stability of the prosthesis and enlarged the impingement–free range of motion (ROM) (19–21). Therefore, considering the anatomical and biomechanical changes that occur in RTSA, it can be estimated that maintaining a fixed COR, the stability

of the glenosphere–baseplate–bone interface, is the most important factor to maintain the stability of the implant.

1.2. Purpose of Research

The original indication of RTSA was irreparable rotator cuff tear and/or rotator cuff arthropathy in older patients (22), however, as prosthesis, surgeons' experience and related surgical skills have improved, the indication of RTSA is expanded to the various disease of glenohumeral joint; complicated proximal humeral fracture, revision shoulder surgery, severe glenoid bone loss including rheumatoid arthritis or osteoarthritis, and tumor (23). Therefore, the operation rate of RTSA is also rapidly increased (24).

Fortunately, the longevity of the RTSA was favorable. The lifespan of an implant at a 10-year follow-up is reportedly up to 90% (25). However, glenoid implants are most commonly associated with complications (26), and these are most likely related to a technical errors (27, 28). Therefore, considering the design characteristics of RTSA, stable initial fixation of the glenoid baseplate is required to achieve favorable functional outcomes and longevity (28).

The glenoid baseplate is fixed to the glenoid vault, which is defined as a conical endosteal structure within a boundary starting from the articular surface of the glenohumeral joint, extending medially to the scapular spine (29). Conventionally, the central fixator of the baseplate is frequently inserted through the point where the vertical and horizontal axes of the glenoid intersect (conventional insertion site, CIS). However, evidence suggesting that CIS is the point of the glenoid vault with the optimal bone stock is scanty. Furthermore, previous studies have reported conflicting results for the insertion point of the baseplate where the depth of

the glenoid vault is the longest (30, 31). Rispoli et al. have argued that the center point of the glenoid vault is slightly anterior and inferior to the center point projected from the surface of glenoid (31), while Matsuki et al. have reported that the depth of the glenoid vault is longer in the posterior portion of the glenoid than the anterior glenoid (30).

Moreover, these previous studies (30, 31) did not consider the fixation force provided by peripheral screws. Although central fixation is considered the most important element in baseplate stability, the number and/or length of the peripheral screw can affect the fixation force of the baseplate (32, 33). Roche et al. have presented that baseplate with 4 or more peripheral screws have been fixed more stable than baseplate fixed with 2 peripheral screws, and longer peripheral screws could provide a greater fixation force (33). Therefore, considering clinical use, we assumed that finding an insertion site where the baseplate can obtain the strongest fixation force within the range where the four peripheral screws can be completely fixed was important.

Moreover, several previous studies have reported the necessity of a smaller size baseplate in the East Asian population (34–36). Our previous studies have presented that the size of the glenoid was significantly smaller in the East Asian population than in the North American cohort (all $p < 0.05$) (37), and have reported that the inappropriate insertion of the central fixator of the glenoid baseplate frequently occurred in the patient with a small glenoid (34). Therefore, we considered that the anatomic information regarding the optimal insertion site of the glenoid baseplate is necessary to achieve the firm initial fixation and the durable longevity of the RTSA, especially in the patient with small glenoid.

We hypothesized that the overlapped volume between the glenoid vault and the central fixator of the glenoid baseplate is different according to the insertion site of the baseplate. To evaluate the optimal insertion site, we measured the volume of overlapped bone stock of the glenoid vault and the central fixator of the baseplate using three-dimensional volumetric measurement.

Chapter 2. Body

2.1. Materials and methods

2.1.1. Sample size calculation

To the best of the authors' knowledge, there were no previous studies that evaluated the optimal insertion site of the glenoid baseplate using three-dimensional volumetric measurements for overlapped volume between the glenoid vault and the central fixator of the baseplate. Therefore, we calculate the minimal sample size using Matsuki et al.'s previous literature which evaluates the depth of the glenoid vault according to the insertion sites of the baseplate (30).

In their study, the depth of the glenoid vault was measured at 77 points, within the range of 6 mm anterior, 6 mm posterior, 10 mm superior, and 10 mm inferior from the CIS by 2 mm interval (30). However, we considered that a 10 mm deviation from the CIS is too large for clinical application, therefore, we elected the 49 insertion points within the range of 6 mm anterior, posterior, superior, and inferior from the CIS by a 2 mm interval.

The pooled mean and standard deviation of the glenoid depth within the range of 6 mm from CIS in all directions was 16.7 ± 7.9 mm (30). The depth of the glenoid vault at CIS was 20.9 ± 5.2 mm. The longest depth of the glenoid vault (24.6 ± 6.4 mm) was measured at the inferior 6 mm and posterior 2 mm, and the shortest depth (7.4 ± 6.7 mm) was measured at the superior 6 mm and anterior 6 mm located from the CIS. We have calculated that the

sample size which can distinguish the longest depth of the glenoid vault from the mean depth of the glenoid vault was 15. However, evaluation of the optimal insertion site using a three-dimensional volumetric measure has not been conducted before, therefore, we have determined the sample size as 30 that can fit a normal distribution according to the central limit theorem to obtain sufficient statistical power.

2.1.2. Materials

We retrospectively reviewed 44 consecutive RTSA procedures performed by the senior author (J.H.O.) of the current study between September 2016 and April 2017 under the approval of the institutional review board of the senior author's affiliation (B-2005/611-109). To reduce heterogeneity and measurement errors according to glenoid deformity, including severe glenoid erosion in osteoarthritis, fracture, and/or congenital dysplasia, we excluded cases of revision RTSA (3 cases), severe proximal humeral fracture (1), with a history of previous surgery and/or fracture on the ipsilateral shoulder (8), or of severe glenoid wear that needed bone graft (2). Therefore, a total of 30 RTSA cases were finally included in this study.

2.1.3. Imaging protocol and 3D reconstruction process

Preoperative computed tomography (CT) images were captured using a 64-channel multidetector CT (Brilliance 64; Philips, Best, Netherlands) without contrast (detector collimation 0.612–0.625 mm; table speed 53–313 mm/s; slice thickness 0.67 mm; reconstruction interval 0.34 mm; effective tube current-time product 156–338 mAs; tube voltage 120–140 kVp; and matrix size

512 × 512). Images covered the entire scapula.

Image evaluation and three-dimensional (3D) reconstruction of CT were independently performed and repeated by two shoulder fellowship-trained orthopedic surgeons (H.J.J. and M.G.J.) with at least a 3-week interval between analyses.

The depth of the glenoid vault was measured at the level of the CIS in axial view using the '3D cursor function' of the G3 Picture Archiving and Communication System (G3 PACS; Infinitt, Seoul, Republic of Korea) to determine the length of the virtual central peg (34). When marking the specific point at the sagittal view with the '3D cursor function', this point is also automatically marked in axial and coronal views (Figure 1).

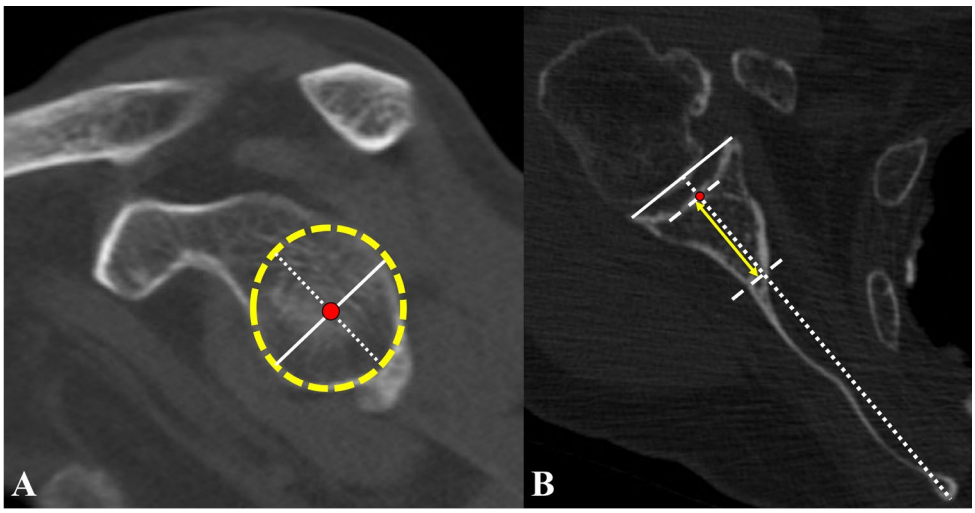

Figure 1. Depth of the glenoid vault. (A) The best-fit circle (yellow, dashed circle) which includes the anterior and posterior end of the glenoid was marked at the sagittal view. The center of the best-fit circle, where the line connecting the anterior and posterior end of the glenoid (white, solid line) was evenly divided, was marked as the conventional insertion site (CIS, red point). (B) Draw the line connecting the anterior and posterior end of the glenoid (white, solid line), and mark the bisecting line (white, dotted line) starting from the medial pole of the scapular spine. Measure the depth of the glenoid vault (yellow, double arrow line) parallel to the bisecting line (white, dotted line).

The entire scapula was three-dimensionally reconstructed using a commercially available program (38-40) (Mimics version 20.0, Materialise, NV, Belgium). Segmentation of the scapula was semi-automatically performed using a 'new mask function' with a preset Hounsfield unit (HU), which included cancellous and cortical bones (range 148-3071). By adjusting the window, the region of interest (ROI) could be set to include the entire scapula, and unnecessarily included humerus and clavicle were removed using the 'split mask function'. Large osteophyte was excluded using the 'edit mask function' manually. Sequentially, the 'smooth mask function' was conducted to clean the extraneous voxel without losing anatomy (41, 42). Three-dimensionally reconstruction was performed using the 'calculate part function', and we smoothed the reconstructed scapula (Figure 2) using the 'smooth object function (smooth factor 0.4, iteration 4)' and 'wrap function (smallest detail 0.2 mm, gap closing distance 1 mm) to avoid measurement error caused by small osteophyte (41, 42).

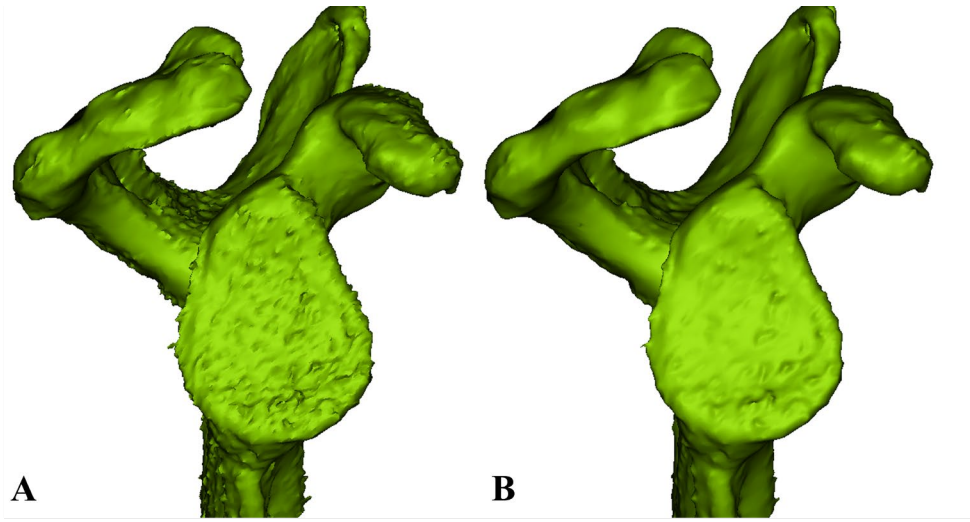

Figure 2. Smoothing operation of the reconstructed scapula. (A) Before smoothing the operation of the scapula, the surface of the scapula looks coarse and unrefined. (B) After smoothing operation using 'smooth object function' and 'wrap function', the glenoid surface looks refined and small osteophytes are automatically removed.

However, the 3D-reconstructed scapula created using this method is problematic in that when the central peg is inserted in the posterior portion of the glenoid, it penetrates both the glenoid vault and the scapular spine. Therefore, to eliminate the error of the central peg being overlapped with the scapular spine, the 3D reconstruction of the glenoid vault, excluding the scapular spine, was performed semi-automatically using the same function and HU (Figure 3).

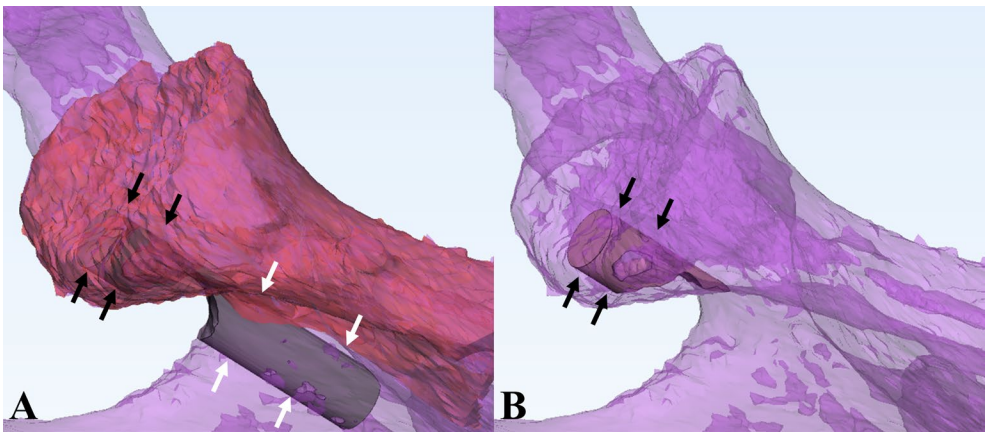

Figure 3. Three-dimensional (3D)-reconstructed anatomical structures and simulated central peg. (A) 3D reconstruction of the entire scapula (violet) and glenoid vault (red). If the scapular spine is not subtracted during the calculation of overlapped volume between the simulated central peg (grey) and glenoid vault, the simulated central peg penetrates both the glenoid vault (black arrow) and scapular spine (white arrow), and overlapped volume is overestimated due to the overlapped area between the central peg and scapular spine (white arrow). (B) Therefore, the authors calculated the overlapped volume using the simulated central peg and 3D-reconstructed glenoid vault. The final version of the overlapped area between the central peg and glenoid vault is presented (black arrow).

Materialise 3-matic Medical (version 12.0, Materialise, NV, Belgium) was used to evaluate the anatomical characteristics. Superior, inferior, anterior, and posterior ends of the glenoid rim where the maximal length of the vertical axis (VA) and horizontal axis (HA) were identified on the en-face view of the 3D-reconstructed glenoid. Subsequently, CIS was marked at the intersection point of the vertical and horizontal axes of the glenoid (31). The medial pole (MP) was also noted on the 3D-reconstructed scapula. Central peg inclination was defined as the angle between the VA and the central axis (CA) connecting MP and CIS, and the glenoid version was defined as the angle between HA and CA (Figure 3). The axis of the scapular spine (SA) was defined as a line connecting MP and the distal 1/3 point of the scapular spine where the scapular spine was equally bisected vertically. To decrease measurement error, SA was drawn at the point where the anterior and posterior ends of the glenoid overlapped entirely (Figure 4).

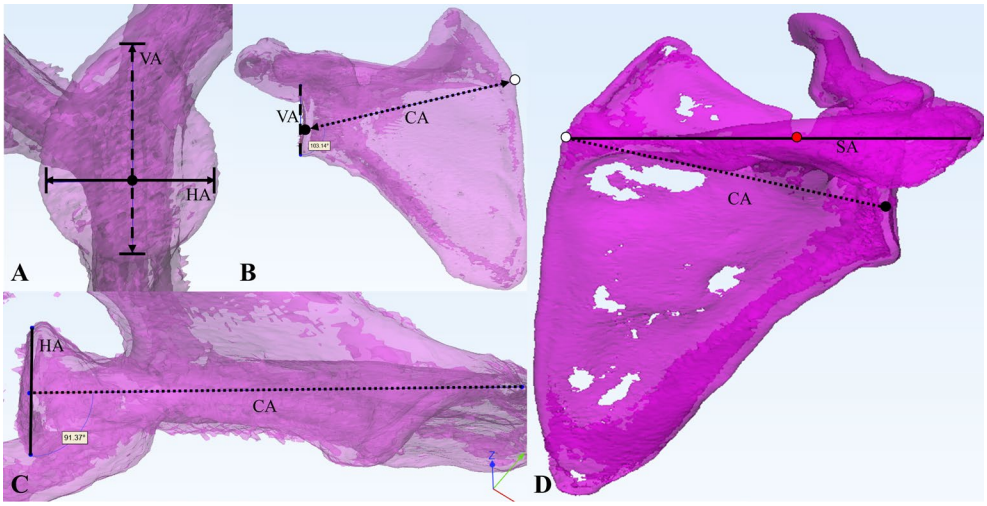

Figure 4. Measurement process. (A) Superior, inferior, anterior, and posterior ends of the glenoid rim where the maximal length of the horizontal axis (HA, straight line) and vertical axis (VA, dashed line) are noted in the en-face view of the 3D-reconstructed glenoid. Subsequently, the conventional insertion site (CIS, black dot) is marked where the vertical and horizontal axes of the glenoid intersect. (B) The medial pole (MP, white dot) is marked on the 3D-reconstructed scapula image. Central peg inclination was defined as the angle between the VA (dashed line) and central axis (CA, dotted line) connecting MP and CIS (black dot), and inclination is measured at the point that optimally overlapped the anterior and posterior ends of the glenoid rim. (C) The glenoid version is defined as the angle between HA (straight line) and CA (dotted line), and the version is measured from the point of view that optimally overlapped the superior and inferior ends of the glenoid rim. (D) The scapular spine bisecting point (BP, red dot) at distal 1/3 of the scapular spine, which equally bisects the scapular spine vertically, is marked on the 3D-reconstructed scapula image. The axis of the scapular spine (SA, straight line) is defined as the line connecting the MP and BP.

To achieve firm fixation of the glenoid baseplate, peripheral screws also played an important role, and, to evaluate the optimal insertion site, we considered that baseplate should be inserted where all peripheral screws could be fully engaged in the glenoid vault. Therefore, we defined the safe transference margin (STM) of the baseplate as the distance at which the outermost part of the peripheral screw hole does not exceed the end of the glenoid rim in four directions from the CIS: superior, inferior, anterior, and posterior. To evaluate the STM, we measured the diameter of a virtual circle based on that of the outermost part of the peripheral screw hole (Figure 5) of several baseplates (Comprehensive®, Zimmer-Biomet, Warsaw, IN, USA; Coralis™, Corentec, Seoul, Republic of Korea; DELTA XTEND™, DePuy-Synthes, Warsaw, IN, USA; Trabecular Metal™ reverse shoulder system, Zimmer-Biomet, Warsaw, IN, USA). Among the four prostheses, the Comprehensive® had the largest diameter (23 mm), followed by Coralis™ 21.9 mm, DELTA XTEND™ 21.2 mm, and Trabecular Metal™ 20 mm. Therefore, we used data from the Comprehensive® to determine the STM. Distances from the CIS to the four points at the superior, inferior, anterior, and posterior ends of the glenoid rim were measured; the radius of the virtual circle of the outermost part of the peripheral screw hole was then subtracted from each measurement to calculate the STM (Figure 5).

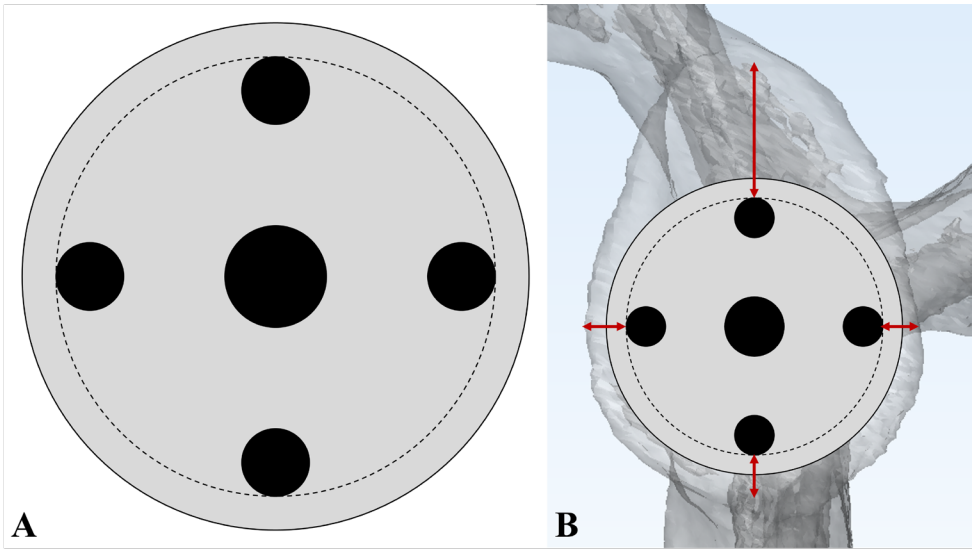

Figure 5. A conceptual diagram of a virtual circle with the diameter of the outermost part of the screw hole for the peripheral screw and the safe transference margin (STM). (A) The single greater central circle represents the central peg and/or screw, and 4 smaller circles represent peripheral screw holes. The radius of the virtual circle with the diameter of the outermost part of the peripheral screw holes (dashed line) is measured to evaluate the STM of the glenoid baseplate. (B) STM is defined as the distance between a virtual circle (dashed line) and the margin of the glenoid rim at the superior, inferior, anterior and posterior direction (red, double arrow line).

The central peg was simulated with the shape of the cylinder with a diameter of 6.5 mm and a length of 35 mm. It was created using the ‘create cylinder’ function. At first, the direction of the central peg was determined using the ‘2 points’ method connecting CIS and MP, and then the length of the central peg was limited to 35 mm in the ‘axis’ method without changing the direction of the central peg. Finally, a simulated central peg was inserted into CIS along the CA (Figure 6B), and the simulated central peg and 3D reconstructed glenoid vault were duplicated 49 times.

To determine the optimal insertion site for the baseplate, simulated central pegs were inserted along the CA from 49 points up to a distance of 6 mm at 2−mm intervals anteriorly, posteriorly, superiorly, and inferiorly from the CIS (Figure 6A). We move the duplicated central peg at a determined distance using the ‘interactive translate’ function. ‘Screen coordinate system’ and ‘translate step’ functions in ‘interactive translate’ made moving the central peg 2 mm interval without changing direction possible. As we considered that the central peg could not be fixed outside the surface of the glenoid, it was located parallel only along the level of the glenoid surface at the CIS, and we assumed that this parallel arrangement of central pegs represents the reaming of the glenoid surface during the preparation of glenoid (Figure 7).

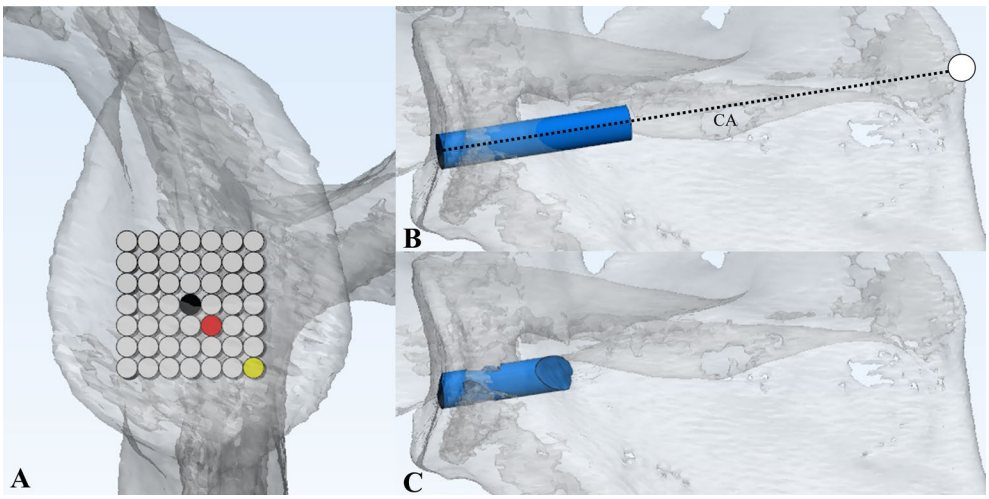

Figure 6. (A) Insertion sites. A simulated central peg is inserted along 49 points up to a distance of 6 mm at 2-mm intervals from the conventional insertion site (CIS, black dot) anteriorly, posteriorly, superiorly, and inferiorly. While the insertion site located 2 mm inferior and 2 mm posterior from the CIS (I2P2, red dot) had the highest overlapped volume, the insertion site located 6 mm inferior and 6 mm posterior from the CIS (I6P6, yellow dot) had the least overlapped volume. (B) A simulated central peg (blue) is inserted in the CIS. A simulated central peg is inserted along the central axis (CA, dotted line), connecting the CIS to the medial pole (white dot). (C) After conducting the boolean intersection function, only the overlapped area (blue) between the simulated central peg and the glenoid vault remains. This represents the amount of glenoid bone stock along the passage of the central peg.

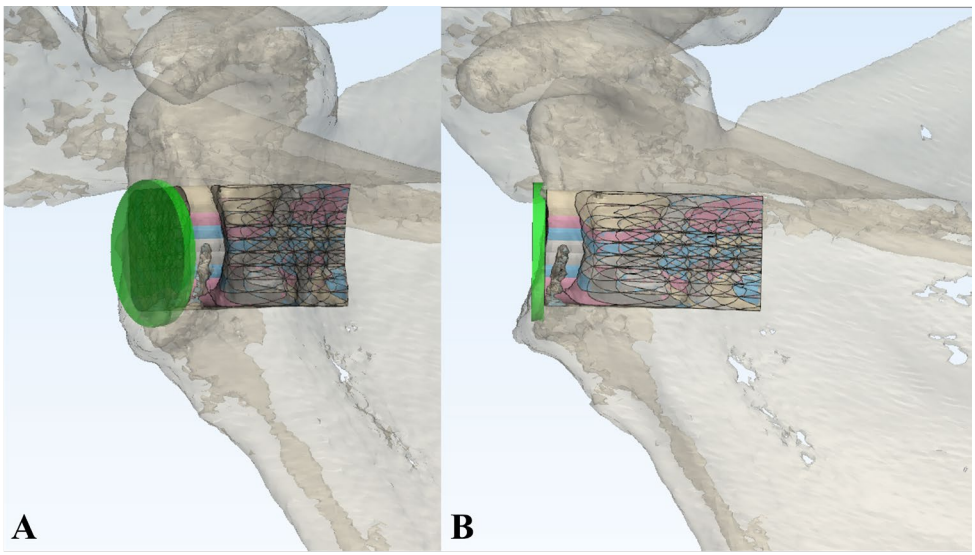

Figure 7. Combined image of the overlapped volume between the glenoid vault and the simulated central peg at every insertion site. (A) The simulated baseplate (transparent green cylinder) and the overlapped area between the glenoid vault and the simulated central peg are presented in the image. (B) In the coronal view, simulated central pegs are inserted parallel to the simulated baseplate. The parallel arrangement of the central pegs represents the reaming of the glenoid surface during the preparation of the glenoid.

Subsequently, the volume of the overlapped area between each simulated central peg and the glenoid vault, which represents the amount of glenoid bone stock along the passage of the central peg, was automatically calculated using the 'boolean intersection' function, which subtracted the non-overlapped area between the central peg and glenoid vault (Figure 6). The overlapped volume was then compared according to each insertion site to elucidate the optimal insertion site. Sequentially, to evaluate the volumetric difference according to the insertion site, we grouped the insertion sites according to the mean overlapped volume by 100 ml: group 1 (>750 ml), group 2 (>700 ml), group 3 (>600 ml), group 4 (>500 ml), and group 5 (≤500 ml).

We also measured the length of the peripheral screws. The peripheral screw was simulated as the cylinder with a diameter of 4.75 mm and a length of 35 mm. It was inserted 9.125 mm away from the CIS and optimal insertion site where the overlapped volume between the glenoid vault and central peg was the largest. To minimize the measurement error, it was inserted parallel to the central peg. The overlapped portion between the glenoid vault and the peripheral screw was automatically simulated using the 'boolean intersection' function in the same manner as the central peg. However, to increase the clinical relevance, we measure the length of the overlapped portion, not the volume (Figure 8). The length of the peripheral screw was measured along the long axis passing through the center of the cylinder.

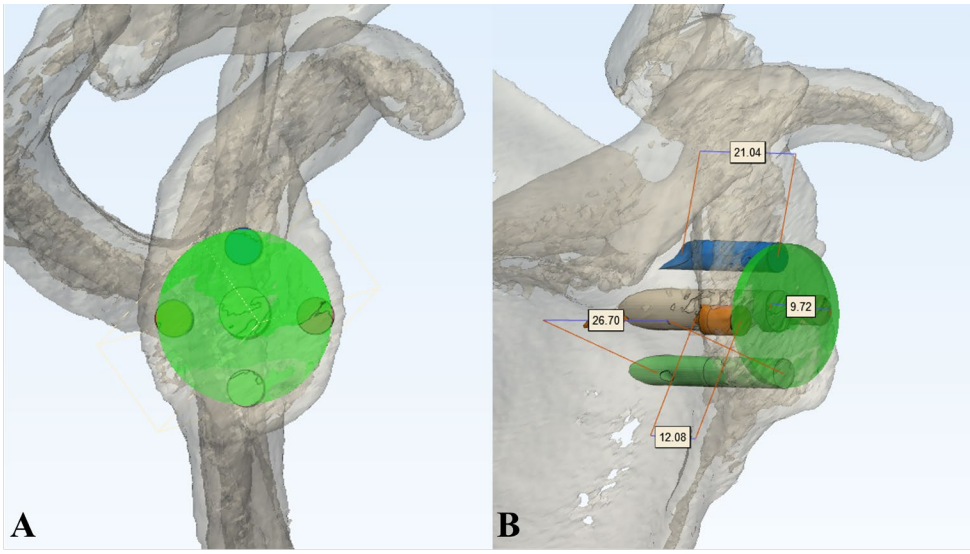

Figure 8. Simulation of the peripheral screw. (A) The boundary of the virtual circle (transparent green cylinder) represents the diameter of the outermost part of the screw hole for the peripheral screw in the baseplate, and its diameter is 23 mm. The diameter of the peripheral screws is 4.75 mm. To coincide the boundaries of the virtual circle and the peripheral screws, peripheral screws were inserted 9.125 mm superiorly, inferiorly, anteriorly, and posteriorly away from the conventional insertion site, respectively. (B) To minimize the measurement error, peripheral screws are inserted parallel to the central peg. After applying the boolean intersection function, the length of the overlapping portion between the glenoid vault and each peripheral screw is measured.

2.1.4. Statistical analysis

All statistical analyses except sample size calculation were conducted using IBM SPSS Statistics, version 22.0 (IBM Corp., Armonk, NY, USA), and the sample size was calculated with the G*Power version 3.1.9.7 (Universität Kiel, Germany). The distribution of data composition was evaluated using the Kolmogorov-Smirnov normality test. Where appropriate, Pearson's or Spearman's correlation test was performed to evaluate the correlation between patients' demographics and anatomical measurements. The one-way analysis of variance (ANOVA) or Kruskal-Wallis test was conducted to discriminate the overlap volume difference between the simulated central peg and glenoid vault based on the optimal insertion site. Paired T-test or Mann-Whitney U test was applied to compare the length of each peripheral screw between CIS and the optimal insertion site. Cronbach's alpha test was performed to evaluate the inter-class and intra-class correlations. All statistical analyses were performed on both sides, and the significance level was set at a p-value of 0.05.

2.2. Results

2.2.1. Demographics

Two men and 28 women, with a mean age of 73.3 ± 5.5 years, were included in this study. The mean height and weight were higher in men (height 170.8 ± 4.0 vs. 149.1 ± 4.6 cm, p = 0.005; weight 72.6 ± 12.1 vs. 58.3 ± 6.7 kg, p = 0.041). However, body mass index (BMI, 26.1 ± 2.9 kg/m2) was not significantly different between sexes (24.8 ± 3.0 vs. 26.2 ± 3.0 kg/m2, p = 0.451). The mean T-score of bone mineral density was -2.3 ± 0.9 and was not also significantly different between the sexes (-1.9 ± 0.7 vs. -2.3 ± 1.0, p = 0.547). Of the 30 included RTSA patients, 2 had received treatment for cuff tear arthropathy, 10 for irreparable rotator cuff tear with osteoarthritis, and 18 for irreparable rotator cuff tear without osteoarthritis; all of them were classified as Walch type A1 [10].

2.2.2. Reliability

The inter- and intra-class correlations of each assessor were evaluated using the depth of the glenoid vault, height and width of the glenoid in the en-face view, inclination of the central peg, and version of glenoid in the 3D-reconstructed scapula, as well as the volume of the overlapped area between the simulated central peg and glenoid vault. The inter- and intra-class correlation of each assessor were higher than 0.9 for all measured variables (all $p < 0.001$, Table I). Therefore, the average value of each measurement was used in further analyses.

Table I. Interclass and intraclass correlations of each assessor

Anatomic marker	Interclass correlation	Significance
Vault depth	0.966 (0.900–0.989)	< 0.001*
Assessor A	0.977 (0.952–0.989)	< 0.001*
Assessor B	0.963 (0.894–0.987)	< 0.001*
Glenoid height	0.957 (0.877–0.985)	< 0.001*
Assessor A	0.982 (0.962–0.991)	< 0.001*
Assessor B	0.969 (0.912–0.990)	< 0.001*
Glenoid width	0.936 (0.822–0.978)	< 0.001*
Assessor A	0.972 (0.942–0.987)	< 0.001*
Assessor B	0.967 (0.902–0.989)	< 0.001*
Central peg inclination	0.931 (0.808–0.976)	< 0.001*
Assessor A	0.985 (0.968–0.993)	< 0.001*
Assessor B	0.973 (0.921–0.991)	< 0.001*
Glenoid version	0.964 (0.894–0.988)	< 0.001*
Assessor A	0.971 (0.939–0.986)	< 0.001*
Assessor B	0.979 (0.937–0.993)	< 0.001*
Volume†	0.903 (0.888–0.916)	< 0.001*
Assessor A	0.974 (0.948–0.987)	< 0.001*
Assessor B	0.941 (0.935–0.947)	< 0.001*

Data are presented as mean (95% confidence interval).

† Volume means the 3-dimensionally reconstructed volume of the intersectional area between the simulated central peg and glenoid vault.

*Statistically significant.

2.2.3. Anatomic measurements

The mean depth of the glenoid vault was 25.5 ± 3.0 mm (range 19.3–31.5), and a sex-specific difference was not observed (26.9 ± 1.8 for men vs. 25.4 ± 3.1 for women, p = 0.607). The length of the simulated central peg was determined to be 35 mm, due to the maximum value of depth of the glenoid vault being 31.5 mm. The mean glenoid height was 33.5 ± 1.9 mm, and it was not statistically different according to sex (35.9 ± 1.1 for men vs. 33.4 ± 1.9 for women, p = 0.092). The mean glenoid width was 26.7 ± 1.9 mm and was significantly larger in men (30.8 ± 1.9 for men vs. 26.4 ± 1.6 for women, p = 0.005). Central peg inclination was 9.8° ± 4.4° (7.3° ± 3.1° for men vs. 10.0° ± 4.5° for women, p = 0.414), and the glenoid version was retroverted at 1.6° ± 4.7° (retroversion 2.7° ± 2.3° for men vs. retroversion 1.6° ± 4.9° for women, p = 0.662). The mean difference between CA and SA was 12.7° ± 2.2° (11.0° ± 0.2° for men vs. 12.9° ± 2.2° for women, p = 0.331).

Patient height correlated with the height (r = 0.627, p < 0.001) and width (r = 0.505, p = 0.004) of the glenoid. However, the depth of the glenoid vault (r = 0.119, p = 0.532), central peg inclination (r = −0.251, p = 0.181), glenoid version (r = −0.010, p = 0.960), and difference between CA and SA (r = 0.036, p = 0.849) did not show a significant correlation.

2.2.4. Optimal insertion site according to the STM of the baseplate and volumetric measurement

The STM of the superior direction was 9.7 ± 1.9 mm, the inferior direction was 1.8 ± 1.6 mm, the anterior direction was 2.2 ± 0.9 mm, and the posterior direction was 1.6 ± 1.3 mm. The

mean overlapped volume between the simulated central peg and the glenoid vault was 623.0 ± 185.8 ml. Overlapped volume at the CIS was 715.7 ± 162.6 ml (Table 2). The optimal insertion site with the highest overlapped volume was 2 mm inferior and 2 mm posterior from the CIS (I2P2, 765.3 ± 157.5 ml). The least favorable insertion site was 6 mm inferior and 6 mm posterior to CIS (I6P6, 470.6 ± 192.4, Figure 6). The distribution of insertion sites grouped according to the mean overlapped volume by 100 ml suggested that slightly inferiorly and posteriorly located insertion sites had higher overlapped volumes (Figure 9).

Table 2. The overlapped volume between the simulated central peg and glenoid vault according to the insertion sites

	A6	A4	A2	0	P2	P4	P6
S6	482.3 ± 142.5	572.8 ± 139.8	626.6 ± 139.9	680.4 ± 148.3	712.6 ± 166.1	642.5 ± 183.4	493.4 ± 169.2
S4	475.6 ± 130.2	564.9 ± 134.1	627.9 ± 144.8	695.4 ± 156.3	740.4 ± 165.1	685.1 ± 195.2	537.0 ± 192.5
S2	477.5 ± 121.3	565.7 ± 132.8	633.1 ± 151.4	709.5 ± 161.9	757.8 ± 162.6	712.4 ± 198.2	566.1 ± 211.9
0	479.9 ± 116.2	567.7 ± 132.5	637.7 ± 154.4	715.7 ± 162.6	765.1 ± 156.8	726.3 ± 197.2	577.4 ± 224.2
I2	483.4 ± 117.7	571.0 ± 135.3	638.4 ± 159.8	715.3 ± 164.4	765.3 ± 157.5	720.4 ± 193.7	565.8 ± 223.8
I4	487.7 ± 124.0	573.7 ± 139.0	634.0 ± 162.0	707.4 ± 166.3	753.8 ± 158.8	695.2 ± 190.9	529.7 ± 209.7
I6	494.7 ± 130.4	582.3 ± 144.6	639.2 ± 159.5	699.4 ± 158.5	726.2 ± 157.2	647.5 ± 191.2	470.6 ± 192.4

Data are presented as mean ± standard deviation (ml).

S superiorly located from conventional insertion site (CIS), *I* inferiorly located from CIS, *A* anteriorly located from CIS, *P* posteriorly located from CIS, *0* 0 mm located from CIS, *2* 2 mm located from CIS, *4* 4 mm located from CIS, *6* 6 mm located from CIS

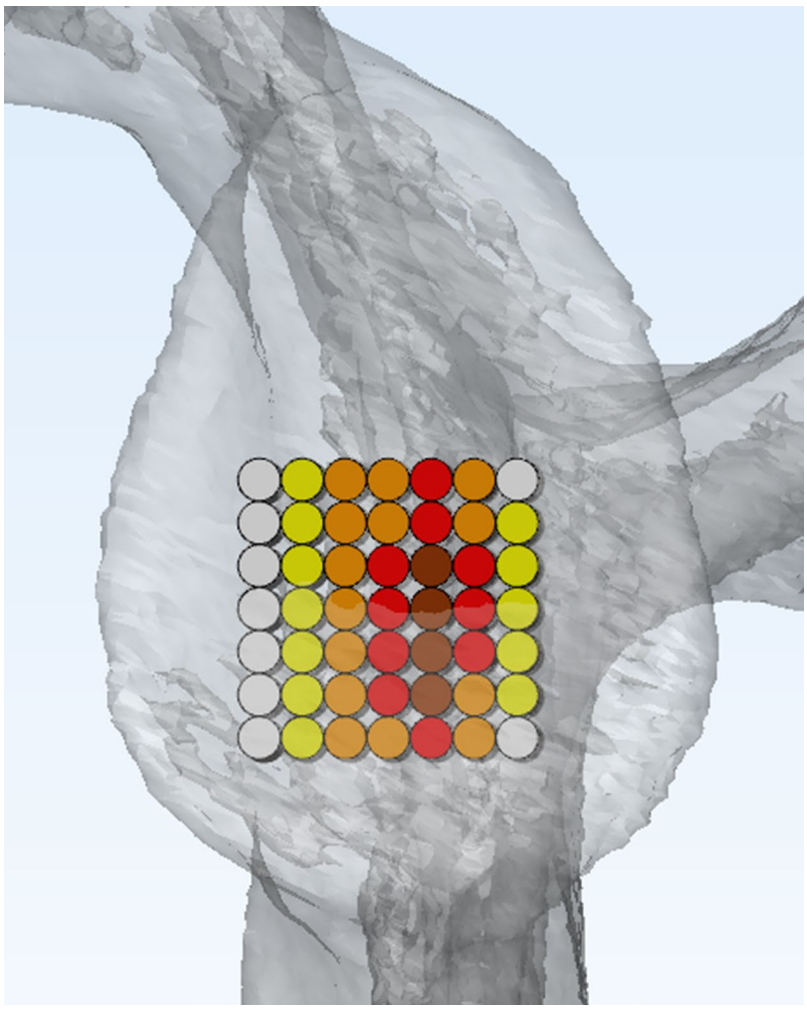

Figure 9. Insertion sites were grouped according to the overlapped volume between the simulated central peg and glenoid vault as below: group 1 (>750 ml, brown), group 2 (>700 ml, red), group 3 (>600 ml, orange), group 4 (>500 ml, yellow), and group 5 (≤500 ml, white).

2.2.5. The length of peripheral screws

The lengths of peripheral screws at CIS were 25.6 ± 4.7 mm (superior), 28.2 ± 4.1 mm (inferior), 14.6 ± 3.2 mm (anterior), and 11.1 ± 3.5 mm (posterior), and the lengths of peripheral screws at the optimal insertion site (I2P2) were 25.5 ± 4.9 mm (superior), 28.3 ± 4.8 mm (inferior), 15.6 ± 4.6 mm (anterior), and 10.7 ± 4.1 mm (posterior), respectively. These were not significantly different between CIS and I2P2 (all $p > 0.05$, Table 3).

Table 3. The length of the peripheral screws according to the insertion site

	Length, mm	Significance
Superior screw		
Conventional insertion site	25.6 ± 4.7	0.800
Optimal insertion site	25.5 ± 4.9	
Inferior screw		
Conventional insertion site	28.2 ± 4.1	0.925
Optimal insertion site	28.3 ± 4.8	
Anterior screw		
Conventional insertion site	14.6 ± 3.2	0.059
Optimal insertion site	15.6 ± 4.6	
Posterior screw		
Conventional insertion site	11.1 ± 3.5	0.317
Optimal insertion site	10.7 ± 4.1	

Data are presented as mean ± standard deviation.

2.3. Discussion

In this study, the optimal insertion site of the baseplate was evaluated using CT and 3D image processing software with excellent inter- and intra-observer reliabilities. This method directly assessed the overlapped volume between the simulated central peg and glenoid vault. The height and width of the glenoid correlated with the height of each patient. The CIS presented a favorable overlapped volume. However, combining the results of volumetric measurements according to insertion sites and the STM, the optimal insertion site to maximize the stability of the glenoid baseplate seemed to be located slightly inferior and posterior. The length of peripheral screws was also not significantly different between CIS and optimal insertion sites.

Firm fixation of the baseplate is a well-known prognostic factor for the outcome of RTSA. Iannotti et al. have shown that the conventional guide pin insertion technique with standard instrumentation alone can often lead to unsatisfactory outcomes (43). Therefore, additional procedures such as patient-specific instruments (PSI) or navigation-guided surgery (NGS) are attempted in severe glenoid wear cases to secure the optimal insertion site for the baseplate. Although PSI and/or NGS have helped achieve favorable outcomes in both clinical and basic research (44-46), these methods are expensive. Performing PSI involves additional costs of developing instrumentation (47). On the other hand, NGS needs a more extended skin incision to attach a marker to the coracoid process (48) and increased procedural time (49) to register glenoid anatomy. Furthermore, follow-up data from long-term follow-up are still absent. Therefore, despite the

theoretical advantage of PSI and/or NGS, these methods cannot be applied to all RTSA cases in actual clinical situations (47).

While the CIS is widely used to achieve strong baseplate fixation, scientific evidence for the optimal insertion site remains insufficient (30, 31, 50). Rispoli et al. reported that the central point at the articular surface was slightly deviated anteriorly and inferiorly from the center point at a depth of 15 mm from the articular surface (31). Conversely, the overlapped volume between the simulated central peg and the glenoid vault was slightly higher in the posterior region in this study, consistent with results from a previous study by Matsuki et al. (30). This difference might be attributed to the different patterns of glenoid wear according to disease entity (osteoarthritis (31) vs. non-arthritis shoulder disease including rotator cuff tear, frozen shoulder, and impingement syndrome (30)) or inter-racial anatomical differences (37).

Several previous studies have reported the necessity of a small baseplate in the East Asian population (34-36). Cabezas et al. have reported that the size of the glenoid is smaller in the East Asian population than in the North American population (37). Therefore, the conventional baseplate which was developed according to the anatomical characteristics of Caucasians seemed to be large in the East Asian population (34). We have reported that the central cage of the elliptical shape baseplate was not appropriately inserted in 31.8% of patients (34). In this study, all cases of central cage exposure from the glenoid vault were superior to posterior in the glenoid vault, and we have recommended that the central cage should be placed lower than the usually targeted insertion point, especially in patients with a small glenoid (34). However, although we have reported the necessity of lowering the baseplate insertion,

we could not have provided the detailed anatomical information which avoids the inappropriate insertion of the baseplate. Therefore, we compared the overlapped volume according to insertion sites by 2 mm interval from CIS and considered that this study provided the theoretical evidence which explains the reason for central cage exposure from the glenoid vault in patients with small glenoids (34).

The methodology of this study seemed similar to that of Matsuki et al.'s previous study (30), however, their method has several limitations. First, Matsuki et al. determined the glenoid plane using the bisecting line which connects the superior and inferior ends of the glenoid. However, as the glenoid has a pear-like morphological shape with wider width in the lower portion, setting the glenoid center based on the line bisecting the vertical axis is more likely to be set above the real anatomical center, and the glenoid inclination might be underestimated. Second, they measured the depth of the glenoid vault from the glenoid surface. However, the baseplate is usually inserted after reaming of the glenoid surface, and we considered that the depth of the glenoid vault might be overestimated as it was measured apart from the center.

Scapular notching, erosion of the inferior scapular neck provoked by impingement of the humeral component during adduction, is a common radiographic finding after RTSA (51). Although, the clinical importance and the optimal treatment of scapular notching are still unclear (52), however, recent meta-analyses presented that functional outcomes were significantly worse in patients with scapular notching after RTSA (53).

To avoid scapular notching, improvements in the design of implants and surgical techniques have been made. Regarding the design of implants, the concept of lateralized RTSA including

glenosphere with a larger diameter and/or lateralized offset and humeral component with lower neck-shaft angle and/or onlay design has been introduced. These modifications in implant design increased the impingement-free ROM, and decrease the incidence of scapular notching (54-59). However, micromotion of glenoid implant caused by the increased shear force in baseplate interface was larger in lateralized glenoid component RTSA (60), and scapular fracture originating from the increased deltoid tension secondary to the overlengthening arm more frequently occurred with the only humeral component (61, 62). Therefore, there has been still no consensus on which design is better, and we have considered that influence of implant design on scapular notching and/or stability of RTSA could not be evaluated in this study. To elucidate these issues, further biomechanical studies or finite element analyses (FEA) are required.

Surgical techniques related to placing the glenoid component are another key to decreasing the scapular notching. To avoid impingement between the inferior scapular neck and humeral component, many orthopedic surgeons insert the glenoid implant with reference to the inferior margin of the glenoid. This surgical technique enables inferior overhang which is the inferior border of the glenosphere extended below the inferior glenoid rim. An inferior overhang could increase the impingement-free ROM and reduce the incidence of scapular notching (51, 63). However, as noted in the current study, the glenoid size can vary according to a patient's height. Therefore, the optimal insertion site based on the inferior margin of the glenoid was considered to vary depending on the size of the glenoid. Since we aimed to determine an optimal insertion site to achieve the most robust central fixation, we assumed that

using CIS as a reference might be better than using an inferior margin to achieve consistent outcomes.

The inferior tilt of the glenoid component is another surgical option to avoid scapular notching (64). We simulated the insertion of the baseplate along the central axis connecting CIS and MP, and it was 9.8° inferior tilted from the glenoid surface. Although we did not measure the volumetric difference according to the tilting angle of the glenoid baseplate, several previous studies have reported that the inferior glenoid baseplate tilt, approximately 10° – 15°, is better than a neutral or superior tilt (28, 65) in clinical and biomechanical aspects. We considered that inferior tilt, obtained through the largest amount of glenoid bone stock, is one of the reasons for the superior clinical and biomechanical results of the inferior glenoid baseplate tilt. Moreover, we considered that the axis of the scapular spine may be used as a surgical landmark to determine the tilting angle of the glenoid baseplate. The mean difference angle between CA and SA was 12.7°, which did not correlate with the height of the patients. Although the tilting angle of the glenoid baseplate may not be accurately measured without NGS, the scapular spine could be palpated easily during surgery. Therefore, we thought that axis of the scapular spine is useful as a palpable landmark to determine the insertion angle for the central peg without NGS.

Another factor affecting the stability of the glenoid baseplate is the size and design of an implant and the fixation force provided by the peripheral screws. As we described above, many orthopaedic surgeons insert the glenosphere concerning the inferior margin of the glenoid to achieve an inferior overhang. However, the baseplate is not solely fixed by the central fixator, but the number and/or the

length of peripheral screws also affect the fixation force of the baseplate (33). Therefore, we thought that the baseplate should be located within the range where all peripheral screws were purchased in the glenoid vault. To maintain stability based on the peripheral screw fixation and maximize the safety of baseplate transference, we calculated the STM using the data from an implant with the largest diameter of the virtual circle originating from the outermost part of the screw holes for peripheral fixation. However, it should also be noted that the STM should differ according to the size and design of an implant. Therefore, we recommend that the surgeons consider each implant's characteristics used in RTSA and that manufacturers should elucidate the detailed specification sheet for implants, including the size and radius of the outermost peripheral screws.

Considering the overlapped volume between the virtual central peg and glenoid vault as well as the STM of the baseplate together, we regarded CIS as a suitable but not optimal insertion site. Our findings suggest that the optimal insertion site of a glenoid baseplate is slightly inferiorly and posteriorly located from the CIS. Furthermore, the length of the peripheral screws was not significantly different between CIS and the optimal insertion site. Although the real length of the peripheral screw can be modified according to the thickness of the baseplate and insertion angle of the peripheral screw, we considered that the information regarding the length of the peripheral screw has clinical value as it has been measured in the same way under equal conditions. Therefore, we estimated that peripheral fixation force may not be different between CIS and optimal insertion sites.

To the best of our knowledge, this is the first study to measure

the stability of the central peg using a volumetric measurement of the overlapped area between the central peg and glenoid vault. As an advantage, our findings are based on simulations of real clinical situations. However, a few limitations of this study should be considered when interpreting our findings.

The process of reconstructing and measuring the anatomical characteristics of 3D-reconstructed images is a time-consuming task. Therefore, the sample size of this study was relatively small. However, we calculated the sample size using the previous study and enrolled a larger number of patients than the calculated sample size to obtain a normal distribution of data. Furthermore, inter- and intra-observer reliabilities were excellent, and our findings are similar to those of a previous study (37). Therefore, we believe that the biases arising from the small sample size were controlled.

Additionally, the difference in sex distribution of participants could be considered a limitation. Although we enrolled participants in this study according to pre-determined criteria, sexual inhomogeneity remained, and sex-specific anatomical differences of the glenoid could have introduced a bias. Therefore, future studies must consider evaluating the sex-specific differences in anatomy.

Interracial anatomical differences might be another limitation. We could not include different racial subgroups in our study. Therefore, future studies based on the methodology of this study should consider enrolling participants with diverse racial backgrounds to account for inter-racial anatomical differences.

The presence of osteoporosis could affect the accuracy of three-dimensional reconstruction. However, dual-energy X-ray absorptiometry of the hip and lumbar spine might not accurately

assess the focal bone mineral density of the bony structure of the shoulder joint (66–68). Furthermore, measurement was conducted at different 49 insertion points, therefore, we considered that although the presence of osteoporosis might act as the cause of measurement error, however, it is unlikely to cause bias. Moreover, the reconstruction process was semi-automatically conducted using preset values originating from the validated, commercially available software (38, 39, 69). Also, the study design was not appropriate to evaluate the accuracy of the three-dimensional reconstruction of glenoids according to the presence of osteoporosis. To resolve this issue, further finite element analysis will be needed.

Moreover, measuring the STM using a single implant may be considered another limitation of this study. Despite best efforts to minimize the STM, we could not guarantee the accuracy of STM for the elliptical and/or non-circular type baseplate. However, a comparison of fixation force according to the design of the baseplate could be conducted through biomechanical study and/or finite element analysis. Furthermore, most manufacturers did not reveal their detailed design sheets; therefore, the authors only used the data of implants wherein an accurate size could be selected to maximize safety and minimize STM size in circular baseplates. For the same reason, we could not evaluate the overlapped volume between the glenoid vault and implants in line with the difference in the design of the central fixator.

Lastly, the concept of scapular notching was not considered in this study. However, scapular notching is caused by multifactorial risk factors including anatomical characteristics of patients (70, 71), design of implants (54–59), and surgical techniques (51, 63). Therefore, we considered that to evaluate the correlation between

scapular notching and the design of implants and/or surgical techniques, biomechanical study or finite element analysis would be more suitable.

Chapter 3. Conclusion

The most abundant point of glenoid bone stock is 2 mm inferiorly and posteriorly located from the CIS. This anatomical finding may be used as a reference to determine the optimal insertion site of baseplates according to the implant of each surgeon's choice, along with several other considerations to reduce scapular notching.

Bibliography

References

1. Dumont GD, Russell RD, Robertson WJ. Anterior shoulder instability: a review of pathoanatomy, diagnosis and treatment. Curr Rev Musculoskelet Med. 2011;4(4):200-7.

2. Lädermann A, Denard PJ, Collin P. Massive rotator cuff tears: definition and treatment. International Orthopaedics. 2015;39(12):2403-14.

3. Bouaicha S, Ernstbrunner L, Jud L, Meyer DC, Snedeker JG, Bachmann E. The lever arm ratio of the rotator cuff to deltoid muscle explains and predicts pseudoparalysis of the shoulder. Bone Joint J. 2018;100-B(12):1600-8.

4. Jeong HJ, Rhee SM, Oh JH. Postoperative New-Onset Pseudoparalysis: A Retrospective Analysis of 430 Consecutive Arthroscopic Repairs for Large to Massive Rotator Cuff Tears. Am J Sports Med. 2018;46(7):1701-10.

5. Parsons IM, Apreleva M, Fu FH, Woo SL. The effect of rotator cuff tears on reaction forces at the glenohumeral joint. J Orthop Res. 2002;20(3):439-46.

6. Burkhart SS, Nottage WM, Ogilvie-Harris DJ, Kohn HS, Pachelli A. Partial repair of irreparable rotator cuff tears. Arthroscopy. 1994;10(4):363-70.

7. Kovacevic D, Suriani RJ, Jr., Grawe BM, Yian EH, Gilotra MN, Hasan SA, et al. Management of irreparable massive rotator cuff tears: a systematic review and meta-analysis of patient-reported outcomes, reoperation rates, and treatment response. J Shoulder Elbow Surg. 2020;29(12):2459-75.

8. Galatz LM, Ball CM, Teefey SA, Middleton WD, Yamaguchi K. The outcome and repair integrity of completely arthroscopically repaired large and massive rotator cuff tears. J Bone Joint Surg Am. 2004;86-A(2):219-24.

9. Jeong HJ, Nam KP, Yeo JH, Rhee SM, Oh JH. Retear After Arthroscopic Rotator Cuff Repair Results in Functional Outcome Deterioration Over Time. Arthroscopy. 2022.

10. Kwon J, Kim SH, Lee YH, Kim TI, Oh JH. The Rotator Cuff Healing Index: A New Scoring System to Predict Rotator Cuff Healing After Surgical Repair. Am J Sports Med. 2019;47(1):173-80.

11. Denard PJ, Ladermann A, Brady PC, Narbona P, Adams CR, Arrigoni P, et al. Pseudoparalysis From a Massive Rotator Cuff Tear Is Reliably Reversed With an Arthroscopic Rotator Cuff Repair in Patients Without Preoperative Glenohumeral Arthritis. Am J Sports Med. 2015;43(10):2373-8.

12. Oh JH, Kim SH, Shin SH, Chung SW, Kim JY, Kim SH, et al. Outcome of rotator cuff repair in large-to-massive tear with pseudoparalysis: a comparative study with propensity score matching. Am J Sports Med. 2011;39(7):1413-20.

13. Baulot E, Sirveaux F, Boileau P. Grammont's Idea: The Story of Paul Grammont's Functional Surgery Concept and the Development of the Reverse Principle. Clin Orthop Relat Res. 2011;469(9):2425-31.

14. Rugg CM, Coughlan MJ, Lansdown DA. Reverse Total Shoulder Arthroplasty: Biomechanics and Indications. Curr Rev Musculoskelet Med. 2019;12(4):542-53.

15. Terrier A, Reist A, Merlini F, Farron A. Simulated joint and muscle forces in reversed and anatomic shoulder prostheses. J Bone Joint Surg Br. 2008;90-B(6):751-6.

16. Ackland DC, Roshan-Zamir S, Richardson M, Pandy MG. Muscle and joint-contact loading at the glenohumeral joint after reverse total shoulder arthroplasty. J Orthop Res. 2011;29(12):1850-8.

17. Ackland DC, Roshan-Zamir S, Richardson M, Pandy MG. Moment Arms of the Shoulder Musculature After Reverse Total Shoulder Arthroplasty. J Bone Joint Surg Am. 2010;92(5).

18. Henninger HB, Barg A, Anderson AE, Bachus KN, Tashjian RZ, Burks RT. Effect of deltoid tension and humeral version in reverse total

shoulder arthroplasty: a biomechanical study. J Shoulder Elbow Surg. 2012;21(4):483-90.

19. Favre P, Sussmann PS, Gerber C. The effect of component positioning on intrinsic stability of the reverse shoulder arthroplasty. J Shoulder Elbow Surg. 2010;19(4):550-6.

20. Clouthier AL, Hetzler MA, Fedorak G, Bryant JT, Deluzio KJ, Bicknell RT. Factors affecting the stability of reverse shoulder arthroplasty: a biomechanical study. J Shoulder Elbow Surg. 2013;22(4):439-44.

21. Berliner JL, Regalado-Magdos A, Ma CB, Feeley BT. Biomechanics of reverse total shoulder arthroplasty. J Shoulder Elbow Surg. 2015;24(1):150-60.

22. Grammont PM, Baulot E. Delta shoulder prosthesis for rotator cuff rupture. Orthopedics. 1993;16(1):65-8.

23. Leafblad N, Asghar E, Tashjian RZ. Innovations in Shoulder Arthroplasty. J Clin Med. 2022;11(10).

24. Best MJ, Aziz KT, Wilckens JH, McFarland EG, Srikumaran U. Increasing incidence of primary reverse and anatomic total shoulder arthroplasty in the United States. J Shoulder Elbow Surg. 2021;30(5):1159-66.

25. Ernstbrunner L, Andronic O, Grubhofer F, Camenzind RS, Wieser K, Gerber C. Long-term results of reverse total shoulder arthroplasty for rotator cuff dysfunction: a systematic review of longitudinal outcomes. J Shoulder Elbow Surg. 2019;28(4):774-81.

26. Favard L, Levigne C, Nerot C, Gerber C, De Wilde L, Mole D. Reverse prostheses in arthropathies with cuff tear: are survivorship and function maintained over time? Clin Orthop Relat Res. 2011;469(9):2469-75.

27. Boileau P. Complications and revision of reverse total shoulder arthroplasty. Orthop Traumatol Surg Res. 2016;102(1 Suppl):S33-43.

28. Gutierrez S, Greiwe RM, Frankle MA, Siegal S, Lee WE, 3rd. Biomechanical comparison of component position and hardware failure in

the reverse shoulder prosthesis. J Shoulder Elbow Surg. 2007;16(3 Suppl):S9-S12.

29. Codsi MJ, Bennetts C, Gordiev K, Boeck DM, Kwon Y, Brems J, et al. Normal glenoid vault anatomy and validation of a novel glenoid implant shape. J Shoulder Elbow Surg. 2008;17(3):471-8.

30. Matsuki K, Sugaya H, Hoshika S, Ueda Y, Takahashi N, Tokai M, et al. Three-dimensional measurement of glenoid dimensions and orientations. J Orthop Sci. 2018.

31. Rispoli DM, Sperling JW, Athwal GS, Wenger DE, Cofield RH. Projection of the glenoid center point within the glenoid vault. Clin Orthop Relat Res. 2008;466(3):573-8.

32. Mourad W, Wiater JM, Wiater BP, Martusiewicz A. Baseplate Options for Reverse Total Shoulder Arthroplasty. Curr Rev Musculoskelet Med. 2020;13(6):769-75.

33. Roche C, Digeorgio C, Yegres J, Vandeven J, Stroud N, Flurin P-H, et al. Impact of screw length and screw quantity on reverse total shoulder arthroplasty glenoid fixation for 2 different sizes of glenoid baseplates. JSES Open Access. 2019;3(4):296-303.

34. Joo Han O, Sanghyeon L, Sung-Min R, Hyeon Jang J, Jae Chul Y. Rationale for Small Glenoid Baseplate: Position of Central Cage within Glenoid Vault (Exactech; Equinoxe; Reverse System). Clin Should Elbow. 2019;22(1):24-8.

35. C. Jha S, Fukuta S, Wada K, Higasino K, Amari-Kita R, Tsutsui T, et al. Optimizing baseplate position in reverse total shoulder arthroplasty in small-sized Japanese females: technical notes and literature review. The J Med Invest. 2016;63(1.2):8-14.

36. Shimozono Y, Arai R, Matsuda S. The Dimensions of the Scapula Glenoid in Japanese Rotator Cuff Tear Patients. Clin Orthop Surg. 2017;9(2):207.

37. Cabezas AF, Krebes K, Hussey MM, Santoni BG, Kim HS, Frankle MA, et al. Morphologic Variability of the Shoulder between the Populations of North American and East Asian. Clin Orthop Surg. 2016;8(3):280-7.

38. Hoenecke HR, Jr., Hermida JC, Flores-Hernandez C, D'Lima DD. Accuracy of CT-based measurements of glenoid version for total shoulder arthroplasty. J Shoulder Elbow Surg. 2010;19(2):166-71.
39. Peltz CD, Divine G, Drake A, Ramo NL, Zauel R, Moutzouros V, et al. Associations between in-vivo glenohumeral joint motion and morphology. J Biomech. 2015;48(12):3252-7.
40. Hoenecke HR, Jr., Hermida JC, Dembitsky N, Patil S, D'Lima DD. Optimizing glenoid component position using three-dimensional computed tomography reconstruction. J Shoulder Elbow Surg. 2008;17(4):637-41.
41. Luu B, Cronauer EA, Gandhi V, Kaplan J, Pierce DM, Upadhyay M. A Finite Element Approach for Locating the Center of Resistance of Maxillary Teeth. J Vis Exp. 2020(158).
42. Cronauer EA. A Finite Element Analysis of Maxillary Centers of Resistance: University of Connecticut; 2017.
43. Iannotti J, Baker J, Rodriguez E, Brems J, Ricchetti E, Mesiha M, et al. Three-dimensional preoperative planning software and a novel information transfer technology improve glenoid component positioning. J Bone Joint Surg Am. 2014;96(9):e71.
44. Nashikkar PS, Scholes CJ, Haber MD. Role of intraoperative navigation in the fixation of the glenoid component in reverse total shoulder arthroplasty: a clinical case-control study. J Shoulder Elbow Surg. 2019;28(9):1685-91.
45. Villatte G, Muller AS, Pereira B, Mulliez A, Reilly P, Emery R. Use of Patient-Specific Instrumentation (PSI) for glenoid component positioning in shoulder arthroplasty. A systematic review and meta-analysis. PLoS One. 2018;13(8):e0201759.
46. Kriechling P, Roner S, Liebmann F, Casari F, Furnstahl P, Wieser K. Augmented reality for base plate component placement in reverse total shoulder arthroplasty: a feasibility study. Arch Orthop Trauma Surg. 2020.
47. Cabarcas BC, Cvetanovich GL, Gowd AK, Liu JN, Manderle BJ, Verma NN. Accuracy of patient-specific instrumentation in shoulder arthroplasty: a systematic review and meta-analysis. JSES Open Access.

2019;3(3):117-29.

48. Barrett I, Ramakrishnan A, Cheung E. Safety and Efficacy of Intraoperative Computer-Navigated Versus Non-Navigated Shoulder Arthroplasty at a Tertiary Referral. Orthop Clin North Am. 2019;50(1):95-101.

49. Verborgt O, Vanhees M, Heylen S, Hardy P, Declercq G, Bicknell R. Computer navigation and patient-specific instrumentation in shoulder arthroplasty. Sports Med Arthrosc Rev. 2014;22(4):e42-9.

50. Jung HJ, Nam T-S, Park D, Jeon I-H. Three-Dimensional Morphometric Analysis of Penetrative Depth and Size of Nonarthritic and Degenerative Arthritic Glenoids: Implications for Glenoid Replacement in Shoulder Arthroplasty. Clin Orthop Surg. 2020;12(2):224-31.

51. Simovitch RW, Zumstein MA, Lohri E, Helmy N, Gerber C. Predictors of scapular notching in patients managed with the Delta III reverse total shoulder replacement. J Bone Joint Surg Am. 2007;89(3):588-600.

52. Friedman RJ, Barcel DA, Eichinger JK. Scapular Notching in Reverse Total Shoulder Arthroplasty. JAAOS. 2019;27(6).

53. Jang YH, Lee JH, Kim SH. Effect of scapular notching on clinical outcomes after reverse total shoulder arthroplasty. Bone Joint J. 2020;102-b(11):1438-45.

54. Lawrence C, Williams GR, Namdari S. Influence of Glenosphere Design on Outcomes and Complications of Reverse Arthroplasty: A Systematic Review. Clin Orthop Surg. 2016;8(3):288-97.

55. Mollon B, Mahure SA, Roche CP, Zuckerman JD. Impact of glenosphere size on clinical outcomes after reverse total shoulder arthroplasty: an analysis of 297 shoulders. J Shoulder Elbow Surg. 2016;25(5):763-71.

56. Berhouet J, Garaud P, Favard L. Evaluation of the role of glenosphere design and humeral component retroversion in avoiding scapular notching during reverse shoulder arthroplasty. J Shoulder Elbow Surg. 2014;23(2):151-8.

57. Torrens C, Guirro P, Miquel J, Santana F. Influence of glenosphere size on the development of scapular notching: a prospective randomized study. J Shoulder Elbow Surg. 2016;25(11):1735-41.

58. Erickson BJ, Frank RM, Harris JD, Mall N, Romeo AA. The influence of humeral head inclination in reverse total shoulder arthroplasty: a systematic review. J Shoulder Elbow Surg. 2015;24(6):988-93.

59. Langohr GD, Willing R, Medley JB, Athwal GS, Johnson JA. Contact mechanics of reverse total shoulder arthroplasty during abduction: the effect of neck-shaft angle, humeral cup depth, and glenosphere diameter. J Shoulder Elbow Surg. 2016;25(4):589-97.

60. Harman M, Frankle M, Vasey M, Banks S. Initial glenoid component fixation in "reverse" total shoulder arthroplasty: a biomechanical evaluation. J Shoulder Elbow Surg. 2005;14(1 Suppl S):162s-7s.

61. Ascione F, Kilian CM, Laughlin MS, Bugelli G, Domos P, Neyton L, et al. Increased scapular spine fractures after reverse shoulder arthroplasty with a humeral onlay short stem: an analysis of 485 consecutive cases. J Shoulder Elbow Surg. 2018;27(12):2183-90.

62. Mayne IP, Bell SN, Wright W, Coghlan JA. Acromial and scapular spine fractures after reverse total shoulder arthroplasty. Shoulder Elbow. 2016;8(2):90-100.

63. Nyffeler RW, Werner CM, Gerber C. Biomechanical relevance of glenoid component positioning in the reverse Delta III total shoulder prosthesis. J Shoulder Elbow Surg. 2005;14(5):524-8.

64. Gutiérrez S, Levy JC, Frankle MA, Cuff D, Keller TS, Pupello DR, et al. Evaluation of abduction range of motion and avoidance of inferior scapular impingement in a reverse shoulder model. J Shoulder Elbow Surg. 2008;17(4):608-15.

65. Dilisio MF, Warner JJ, Walch G. Accuracy of the Subchondral Smile and Surface Referencing Techniques in Reverse Shoulder Arthroplasty. Orthopedics. 2016;39(4):e615-20.

66. Oh JH, Song BW, Kim SH, Choi JA, Lee JW, Chung SW, et al. The

measurement of bone mineral density of bilateral proximal humeri using DXA in patients with unilateral rotator cuff tear. Osteoporosis International. 2014;25(11):2639-48.

67. Oh JH, Song BW, Lee YS. Measurement of volumetric bone mineral density in proximal humerus using quantitative computed tomography in patients with unilateral rotator cuff tear. J Shoulder Elbow Surg. 2014;23(7):993-1002.

68. Jeong HJ, Ahn JM, Oh JH. Trabecular Bone Score Could Not Predict the Bone Mineral Density of Proximal Humerus. J Bone Metab. 2021;28(3):239-47.

69. Asadi Nikooyan A, Van Der Helm FCT, Westerhoff P, Graichen F, Bergmann G, Veeger HEJ. Comparison of Two Methods for In Vivo Estimation of the Glenohumeral Joint Rotation Center (GH-JRC) of the Patients with Shoulder Hemiarthroplasty. PLoS ONE. 2011;6(3):e18488.

70. Arashiro Y, Izaki T, Miyake S, Shibata T, Yoshimura I, Yamamoto T. Influence of scapular neck length on the extent of impingement-free adduction after reverse total shoulder arthroplasty. J Shoulder Elbow Surg. 2022;31(1):185-91.

71. Contreras JJ, Khek P, Ogrodnik C. Glenoid neck length in a healthy population and its association with scapular notching. J Orthop Sci. 2021.

국문 초록

목적: 역행성 인공관절 치환술에서 관절와 치환물의 통상적 삽입 위치(conventional insertion site, CIS)는 관절와의 수직 장축과 수평 장축이 교차하는 부위였다. 그러나 통상적 삽입 위치의 골량이 가장 이상적이라는 이론적 근거는 희박하다. 이에 3차원 영상 재구성을 통한 관절와의 골량의 정량적 부피 측정 방법을 통해 관절와 치환물의 최적의 삽입 위치를 평가하고자 한다.

방법: 연속적으로 행해진 30례의 역행성 인공관절 치환술의 수술 전 컴퓨터 단층 촬영 영상(computed tomography, CT)을 3차원 영상 재구성 프로그램을 통해 분석하고, 마찬가지로 3차원으로 구성한 관절와 치환물의 중심부 고정물을 삽입을 모사하였다. 모사한 중심부 고정물은 관절와의 통상적 삽입 위치를 기준으로 하여 관절와의 수직 장축과 수평 장축을 따라 2mm 간격으로 표기한 격자형의 49개의 지점에서 삽입하였으며, 삽입된 중심부 고정물과 관절와의 골성 구조 간 중첩되는 부분의 부피를 측정하여, 중심부 고정물의 고정에 사용되는 골량을 정량적으로 계산하였다.

결과: 관절와의 깊이는 평균 25.5 ± 3.0 mm (범위 19.3-31.5)였으며, 모사한 관절와 치환물 중심부 고정물과 관절와 간 중첩되는 부분의 부피는 평균 623.0 ± 185.8 ml였다. 중심부 구정물의 고정에 가장 적합한 위치는 기존의 통상적 삽입 위치보다 2mm 하방, 2mm 후방에 위치하였으며, 최적 삽입 위치에서의 골량은 평균 765.3 ± 157.5 ml였다.

결론: 관절와 치환물의 최적의 삽입 위치는 통상적 삽입 위치에 비해서 하방, 후방으로 전위되어 있다. 이러한 해부학적 정보는 각 술자들이 선택한 인공관절 치환물의 삽입에 있어 임상적 기준점으로 사용될 수 있을 것이다.

주요 단어: 관절와 치환물, 역행성 인공관절 치환술, 관절와 치환물의 최적 삽입 위치, 3차원 부피 측정

학번: 2018-35046